



Constitutive relationships and physical basis of fault strength due to flash heating

N. M. Beeler,¹ T. E. Tullis,² and D. L. Goldsby²

Received 14 February 2007; revised 24 June 2007; accepted 29 August 2007; published 10 January 2008.

[1] We develop a model of fault strength loss resulting from phase change at asperity contacts due to flash heating that considers a distribution of contact sizes and nonsteady state evolution of fault strength with displacement. Laboratory faulting experiments conducted at high sliding velocities, which show dramatic strength reduction below the threshold for bulk melting, are well fit by the model. The predicted slip speed for the onset of weakening is in the range of 0.05 to 2 m/s, qualitatively consistent with the limited published observations. For this model, earthquake stress drops and effective shear fracture energy should be linearly pressure-dependent, whereas the onset speed may be pressure-independent or weakly pressure-dependent. On the basis of the theory, flash weakening is expected to produce large dynamic stress drops, small effective shear fracture energy, and undershoot. Estimates of the threshold slip speed, stress drop, and fracture energy are uncertain due to poor knowledge of the average contact dimension, shear zone thickness and gouge particle size at seismogenic depths.

Citation: Beeler, N. M., T. E. Tullis, and D. L. Goldsby (2008), Constitutive relationships and physical basis of fault strength due to flash heating, *J. Geophys. Res.*, 113, B01401, doi:10.1029/2007JB004988.

1. Introduction

[2] Fault slip produces heat per unit area Q equal to the product of shear resistance τ and the total slip δ ; thus heat production is proportional to the slip rate V as

$$dQ = \tau V dt. \quad (1)$$

If fault surfaces are rough, then the normal stress is supported by areas of asperity contact rather than over the entire fault surface area. In this case, the average area of an asperity contact A_c is much smaller than the fault area $A \gg A_c$, and the average contact shear resistance or stress,

$$\tau_c = \tau A / n A_c, \quad (2)$$

is proportionally larger than the macroscopic shear resistance; here n is the number of contacts. Therefore thermal effects such as melting, dehydration or other phase changes resulting from shear heating that may dramatically alter fault strength during rapid slip occur initially at asperity contacts due to the high shear stress $\tau_c \gg \tau$. Rice [1999, 2006] considered the implications of shear induced flash weakening at asperity contacts for fault strength at high sliding velocity. The Rice model, discussed in detail below, assumes a single representative contact dimension (Figure 1), and no shear strength of the product phase.

These assumptions produce abrupt and dramatic weakening and a strongly negative rate-dependent fault strength.

[3] Natural faults have fractal surface roughness [Power and Tullis, 1992] and laboratory faults have a distribution of contact asperity sizes [e.g., Brown and Scholz, 1985; Dieterich and Kilgore, 1996], rather than a single contact dimension as assumed in Rice's model. Rice's model also does not consider nonsteady state evolution of fault strength that may occur during accelerating (weakening) and decelerating (strengthening) slip. In this paper we extend the Rice model to consider faults with lab-like contact size distributions and the evolution of strength with displacement expected from a shear-induced phase change at asperity contacts. We assess the importance of these additional factors and produce a semiempirical constitutive equation suitable for modeling fault strength during dynamic rupture. The model is compared to published lab data and implications for the onset slip speed, melt viscosity, melt thickness, asperity contact dimension, stress drop, slip weakening distance, shear fracture energy, and overshoot for lab and natural faulting are explored.

2. Shear Heating and Friction: Rice's Model

[4] Frictional strength during sliding at constant slip rates less than 100 $\mu\text{m/s}$ and low normal stress in lab experiments is to first-order constant with displacement and with sliding velocity [e.g., Ruina, 1983], suggesting that the real area of asperity contact across the fault is neither displacement nor time-dependent. We therefore assume throughout this study that contact area is independent of displacement and time; this is equivalent to assuming that the size distribution of asperity contacts is stationary in time. For example, consider

¹U.S. Geological Survey, Menlo Park, California, USA.

²Department of Geological Sciences, Brown University, Providence, Rhode Island, USA.

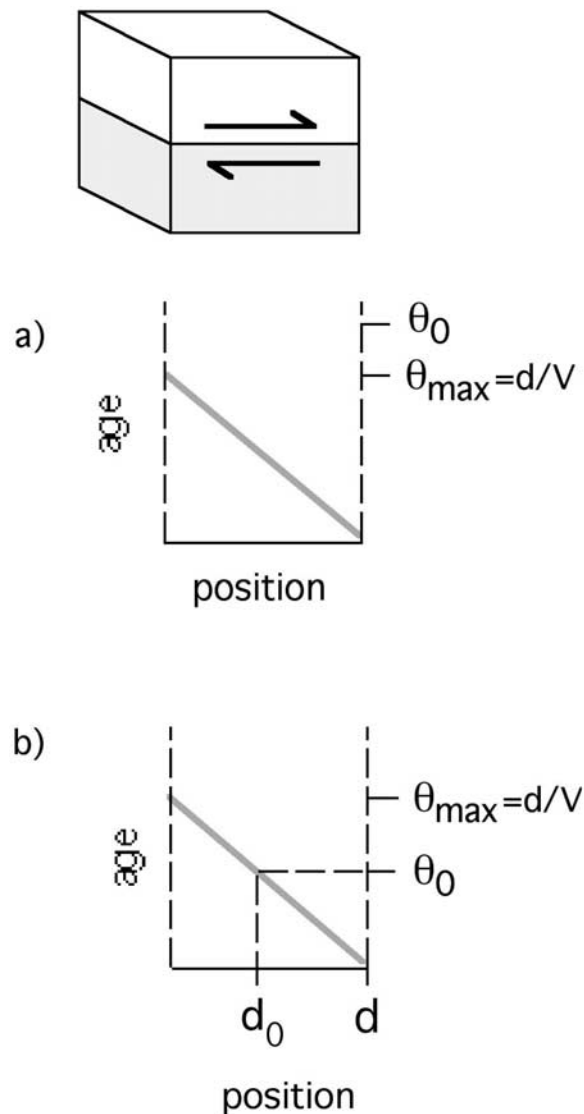


Figure 1. (a) Square contact of dimension d , slid into perfect registry at constant rate V . Plot shows the spatial distribution of time of contact (age) with reference to the lower contacting asperity [after *Tullis et al.*, 1993]. For this case the critical age for weakening θ_0 exceeds the maximum contact age θ_{\max} . (b) Same as in Figure 1a but for $\theta_0 < \theta_{\max}$.

sliding between an array of aligned, identical square asperities at a constant rate V in a direction perpendicular to the asperity edge (Figure 2). A unit cell area of fault surface consists of 2 sets of contacts (4 asperities), one set that is initially in perfect registry and a second set that is initially not in contact (Figure 2). Over displacement equal to the contact edge dimension d , the first set of contacts is incrementally replaced by the second set while the average contact age remains constant. While contact age varies spatially and temporally within an individual contact and differs between contacts, the collective age and the steady state behavior can be represented by a single contact in exact registry (Figure 1a). The maximum contact age at the representative contact is $\theta_{\max} = d/V$ while the average age is half the maximum, $\theta = d/2V$.

[5] To consider thermal weakening at asperity contacts, assume the starting contact strength as given by the classical theory of friction [e.g., *Bowden and Tabor*, 1950]. Friction theory stipulates that asperity contacts yield plastically and the applied contact normal stress σ_c is the material yield strength $\sigma_c = \sigma_y$, as is consistent with recent contact-scale studies of rock friction [*Dieterich and Kilgore*, 1996]. Under these circumstances, as the macroscopic normal stress increases, the real area of contact increases according to $A_c = A\sigma/n\sigma_c$. If the shear resistance of contact junctions is also a material property $\tau_c = S$, the coefficient of friction f , the ratio of macroscopic shear resistance to normal stress, is the ratio of the junction shear resistance to the yield strength

$$f = \frac{\tau}{\sigma} = \frac{S}{\sigma_y}. \quad (3)$$

A friction coefficient approximately independent of normal stress is consistent with experimental data from a wide range of rock types [e.g., *Summers and Byerlee*, 1977; *Byerlee*, 1978].

[6] Large changes in strength induced by shear heating can arise if a low-temperature phase with frictional contact shear strength $\tau_c = S$ at temperature T_f is replaced by a high-temperature phase of different shear strength τ_w . In particular we assume that the transformation occurs instantaneously at a threshold weakening temperature T_b . Under these conditions the critical duration of heating θ_0 required to weaken an asperity contact, equivalent to the critical contact lifetime, can be derived from a heat balance [*Rice*, 1999]. Rice assumes one-dimensional heat conduction and that the shear-generated heat $(1) SV\theta_0$, over the critical duration θ_0 is balanced by the product of the change in thermal energy $\rho\hat{c}(T_b - T_f)$ and the width of the affected

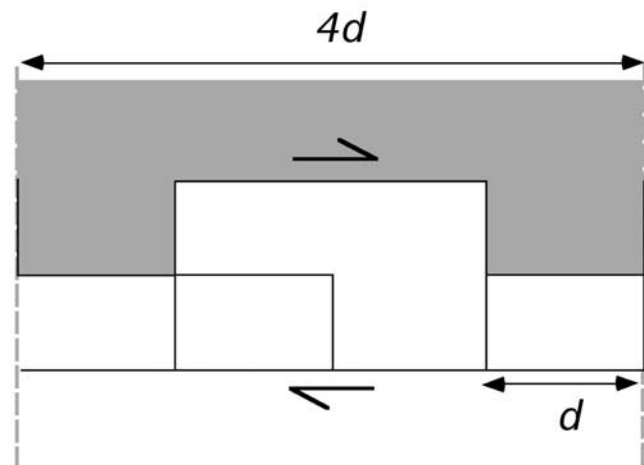


Figure 2. Unit cell of a one-dimensional array of square contacts shown in cross section. The vertical dashed lines are the boundaries of the unit cell. The array is assumed to be repeated to the left and to the right about the array boundaries an infinite number of times. The array has displacement independent contact area. If slid at constant rate, the array has time-independent contact age.

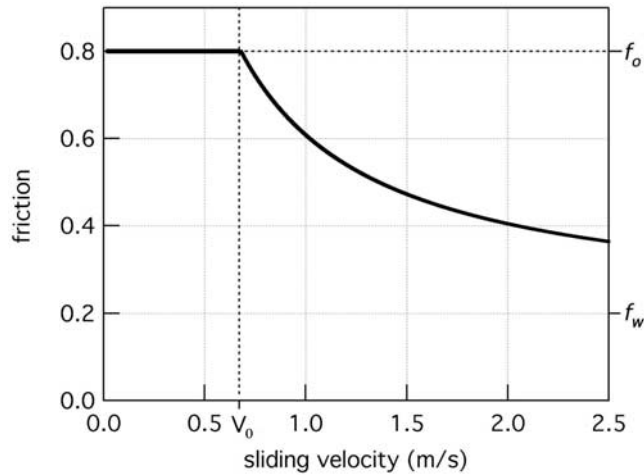


Figure 3. Steady state behavior of the modified Rice model for flash weakening (equation (5)) with $f_o = 0.8$, $f_w = 0.2$, $V_0 = 0.68$ m/s [after *Rice*, 1999].

region $\sqrt{\pi\alpha\theta_0}$, where α is thermal diffusivity, and $\rho\hat{c}$ is the volumetric heat capacity. The critical duration,

$$\theta_0 = \frac{\pi\alpha}{V^2} \left[\frac{\rho\hat{c}(T_b - T_f)}{S} \right]^2, \quad (4a)$$

is the time necessary to weaken at a fixed slip speed. Heating at the asperity contact is further limited by the total slip which has a maximum of the contact dimension d . So, to consider the threshold velocity for weakening V_0 change the V in (4a) to V_0 and substitute into $V_0 = d/\theta_0$, resulting in

$$V_0 = \frac{\pi\alpha}{d} \left[\frac{\rho\hat{c}(T_b - T_f)}{S} \right]^2. \quad (4b)$$

[*Rice*, 1999]. Alternatively, the critical contact dimension for weakening at a fixed sliding velocity is $d_0 = \theta_0 V$,

$$d_0 = \frac{\pi\alpha}{V} \left[\frac{\rho\hat{c}(T_b - T_f)}{S} \right]^2. \quad (4c)$$

[7] To determine an approximate steady state solution for fault strength, for simplicity we first use the geometry of identical square contacts, with reference to Figure 1. If the critical age (4a) is greater than the maximum age then no portion of the contact is weakened and the frictional shear resistance is

$$f = f_o, \quad \theta_0 > \theta_{\max}(V < V_0) \quad (5a)$$

(Figure 1a). However, if the critical age is less than the maximum age, then a portion of the contact is weakened. *Rice* [1999] originally assumed that the weakened portion of the contact has no strength, but this may be too restrictive. Consistent with (3), define a weakened resistance $f_w = \tau_w/\sigma_n$. For a weakened contact, the average steady state shear

resistance is the weighted sum of the weakened $f_w (d - d_0)/d$ and strong $f_o d_0/d$ portions, or

$$f = \frac{d_0}{d} (f_o - f_w) + f_w, \quad \theta_0 < \theta_{\max}(V > V_0) \quad (5b)$$

(Figure 1b). The spatial age construction (Figure 1b) illustrates the identities $d = V\theta_{\max}$ and $d_0 = V\theta_0$ which require

$$f = \frac{\theta_{\max}}{\theta_0} (f_o - f_w) + f_w, \quad \theta_0 < \theta_{\max}(V > V_0). \quad (5c)$$

This can be expressed in terms of velocity using the identity $V = d/\theta_{\max}$ and (4a) for θ_0 as

$$f = (f_o - f_w) \frac{\pi\alpha}{dV} \left[\frac{\rho\hat{c}(T_b - T_f)}{S} \right]^2 + f_w = (f_o - f_w) \frac{V_0}{V} + f_w, \quad \theta_0 < \theta_{\max}(V > V_0). \quad (5d)$$

We refer to (5) as the modified Rice model. If the asperity has effectively no strength in its weakened state, $f_w = 0$, the solution to equation (5d), $f = f_o V_0/V$, is that given by *Rice* [1999] as a steady state solution for flash weakening. For any low value of f_w , flash processes should produce the very strong negative rate dependence of fault strength (5d) [*Rice*, 1999]. An example of this steady state behavior is shown in Figure 3. Laboratory observations possibly resulting from flash heating are data on gabbro from *Tsutsumi and Shimamoto* [1997] (Figure 4a) and for novaculite by D. L. Goldsby and T. E. Tullis (unpublished data, 2003) (Figure 4b). These data indicate V_0 in the range of 0.1 to 0.2 m/s (Figure 4) and some comparison between observations and expectations from the model (5d) is included in section 6.1. The fit to the data suggests that the residual strength is non zero, though additional data are necessary to confirm the behavior at higher slip speeds. It is also possible that the onset of weakening for gabbro is more gradual than a simple threshold; this is expected if the contact population is not well represented by a single dimension and more gradual onsets should be the norm for natural fault surfaces.

3. Contact Populations

[8] Natural fault surfaces are rough over many orders of magnitude [e.g., *Power and Tullis*, 1992] and as noted by *Rice* [1999], for earthquake modeling it is probably not sufficient to represent the contacting asperities across a fault with a single contact dimension. In the case of natural joint surfaces roughness and asperity contact populations are fairly well known [e.g., *Brown and Scholz*, 1985] and can be described by Gaussian or similar distributions. Here we expand the modified Rice model to include the effects of a contact population on the steady state shear resistance.

[9] Consider a fault surface sliding at constant sliding velocity with a distribution of asperity contact sizes characterized by a probability density $P(d)$ (Figure 5a). The distribution of asperity contact sizes is presumed to be

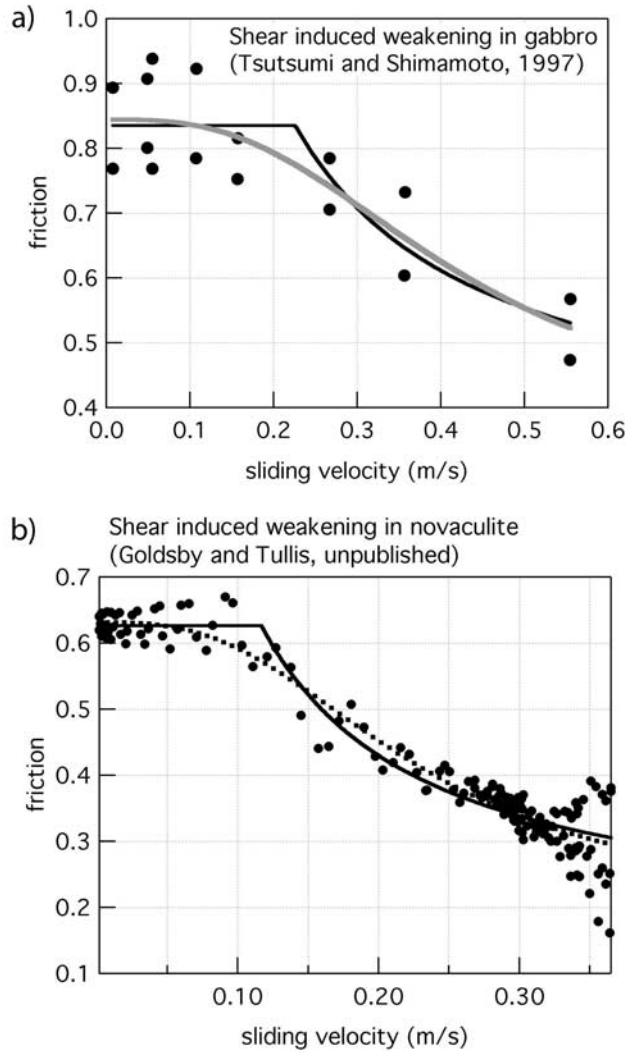


Figure 4. Laboratory fault strength data from high-speed sliding. (a) Gabbro at 1.5 MPa normal stress [Tsutsumi and Shimamoto, 1997] showing a least squares fit using the modified Rice model (solid line), equation (5) with $f_0 = 0.835$, $f_w = 0.32$, and $V_0 = 0.226$ m/s. Also shown is a fit with the empirical equation (7) with $f_0 = 0.84$, $f_w = 0.436$, and $V_0 = 0.2$ m/s (dashed). (b) Novaculite at 5 MPa normal stress (D. L. Goldsby and T. E. Tullis, unpublished data, 2003). Fit with the modified Rice model (solid line) with $f_0 = 0.626$, $f_w = 0.155$, and $V_0 = 0.117$ m/s. Fit with the empirical relation (7) with $f_0 = 0.631$, $f_w = 0.065$, and $V_0 = 0.23$ m/s (dashed line).

stationary in time yielding a steady state frictional resistance $f_{ss}(V)$. That is, the fault surface roughness and asperity population are not altered by wear and the formation of gouge with continued slip. Although such processes do occur and may be important [e.g., Power et al., 1988; Di Toro et al., 2006], they are ignored to simplify the analysis. The contact size distribution is proportional to the age distribution $P(\theta_{\max})$ since $d = V\theta_{\max}$ (Figure 5b). If the contacts are square, aligned, and sliding perpendicular to their edges, individual contact strength varies with size and sliding velocity according to (5d) if $d > d_0$ where d_0 is

defined by (4c). Contact strength is rate-independent (5a) when $d < d_0$. The total strength then is

$$f_{ss} = f_0 \int_0^{d_0} P(d) dd + \int_{d_0}^{\infty} \left[(f_0 - f_w) \frac{d_0}{d} + f_w \right] P(d) dd. \quad (6)$$

Differences between the predictions of (6), which allows for an arbitrary distribution of contact sizes, and those of (5) depend on the specific shape and breadth of the distribution; an example of the steady state strength resulting from a lognormal distribution of contact sizes is shown in Figure 5c. This case was calculated numerically. The onset of weakening occurs at lower sliding velocity than in the Rice model because there are contacts larger than the mean; these weaken at lower sliding velocity. The weakening is gradual because there are only a few large contacts. At higher velocity, the fault is not as weak as in the Rice model because there are contacts much smaller than the mean; at high sliding rates, these maintain a higher strength than the mean and larger size contacts. As the breadth of the distribution decreases, equation (6) approaches the Rice model.

[10] The distributions of asperity contact sizes of natural seismic faults are not well known and they may vary substantially with normal stress [Scholz, 1988]. Even for laboratory fault surfaces, the contact size distribution depends on surface preparation and may vary with shear strain particularly in high-speed, large displacement, high normal stress experiments [e.g., Goldsby and Tullis, 2002]. Present knowledge does not allow extrapolation of laboratory surface roughness data to natural seismic faults. Furthermore, even if contact size distributions were well known, the integral equation (6) is not well suited for use in dynamic calculations of fault slip or in dynamic rupture modeling. Therefore we propose an empirical expression for flash processes which is bounded by the theoretical expectations of the Rice model and our extension of it, and can be used to represent the behavior expected with a distribution of asperity contact sizes (Figure 5c):

$$f = f_w + \frac{f_0 - f_w}{1 + \frac{V}{V_0} \left\{ 1 - \exp \left[- \left(\frac{V}{V_0} \right)^2 \right] \right\}}. \quad (7)$$

[11] The empirical expression (7) may fit the onset of weakening in lab faulting experiments better than the simple model (5) in some cases (Figure 4), however the differences are slight and given the scatter using (7) rather than (5) is probably not warranted for laboratory surfaces (see discussion). For (7) at high velocity and $f_w = 0$, $f \approx V_0/V$ as required by (5) and by the numerical solutions to (6). Furthermore, at low velocity, friction is constant at $f \approx f_0$, again consistent with (5) and (6). As (7) is continuous and differentiable, rather than piecewise, it can be more easily incorporated in dynamic models and combined with constitutive equations for low-speed friction. Additional

flexibility can be introduced by allowing the characteristic velocity in the exponential to be different from V_0 .

4. Nonsteady State Behavior and the Evolution of Contact Age With Slip

[12] Equations (5), (6) and (7) are models of steady state fault strength based on the steady state age of the contact population; however for flash heating and other contact-scale phenomenon, including rate and state friction [Ruina, 1983; Linker and Dieterich, 1992], the average contact age

does not change instantaneously with slip velocity. For example, consider the representative square contact sliding initially at a constant initial rate V_1 (Figure 1). Contact age increases linearly from zero to d/V_1 over the contact. If the sliding velocity is instantaneously changed, the spatial distribution of age over the contact changes systematically with slip δ [Tullis *et al.*, 1993] (Figure 6). This change is reflected in the displacement-dependent change in the average contact age $\hat{\theta}$,

$$\hat{\theta} = \frac{\delta}{d} \left[\frac{\delta}{2V_2} \right] + \frac{d-\delta}{d} \left[\frac{\delta}{V_2} + \frac{d-\delta}{2V_1} \right], \quad 0 < \delta \leq d \quad (8a)$$

$$\hat{\theta} = \frac{d}{2V_2}, \quad \delta > d. \quad (8b)$$

For flash processes, as for lower speed friction, under some circumstances the nonsteady state change in age such as (8) should be included. The distribution of age over an arbitrary contact shape and the displacement dependence of this age can be considered by dividing the contact into chord lengths in the sliding direction [Dieterich and Kilgore, 1996]. Somewhat different behavior results for different contact shapes or if the sliding direction is oblique to the contact edge [Tullis *et al.*, 1993]. At least for simple contact shapes these differences are slight and we do not discuss these further in the present paper.

[13] Significant differences in the evolution behavior result if, instead of a single contact, there is a wide distribution of contact sizes. In general, the displacement-dependent average age for a distribution of aligned square contacts sliding perpendicular to their edges is

$$\hat{\theta}(\delta) = \int_0^{\infty} P(d)\theta(\delta)dd. \quad (9)$$

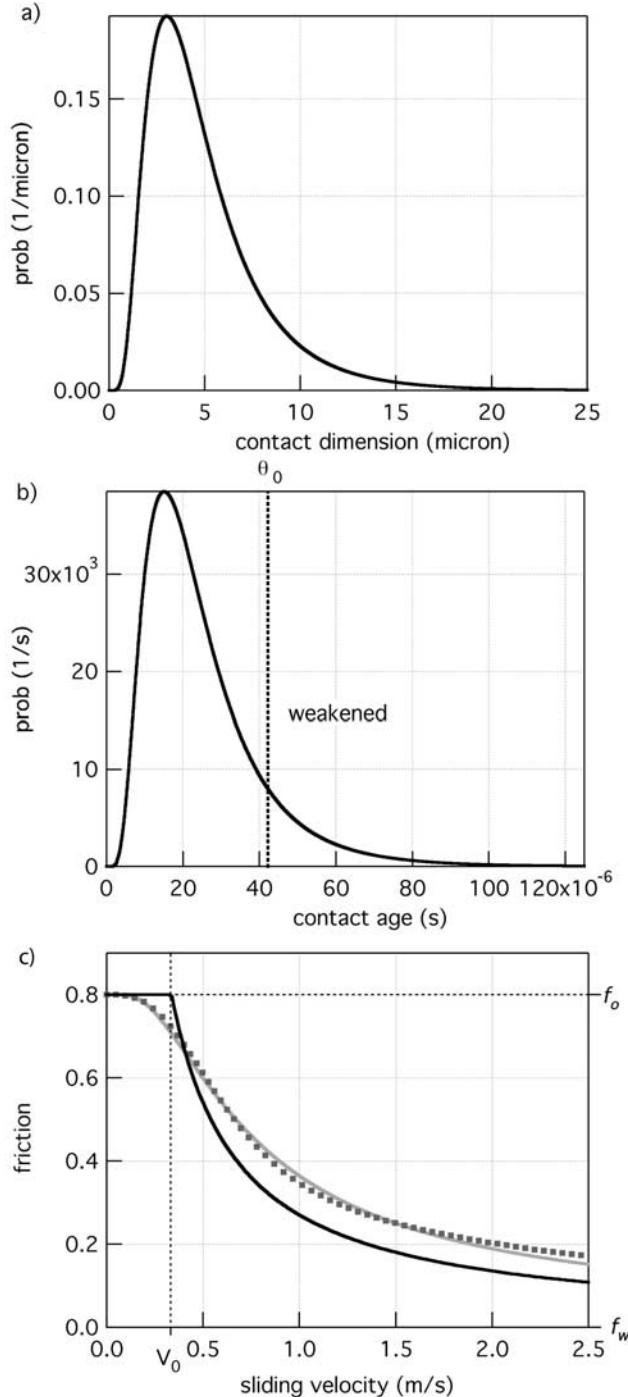
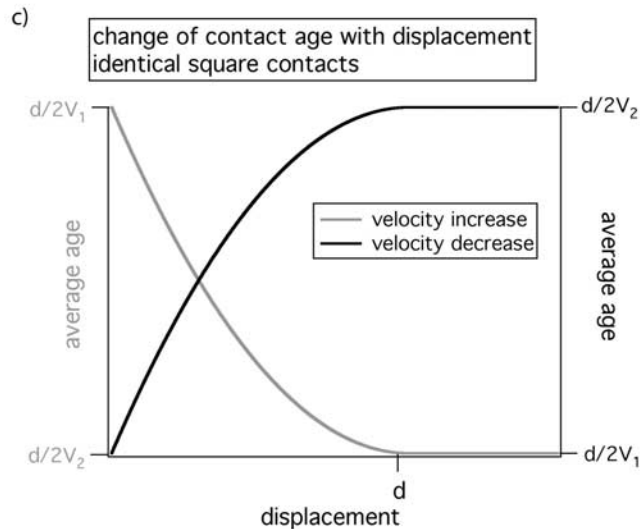
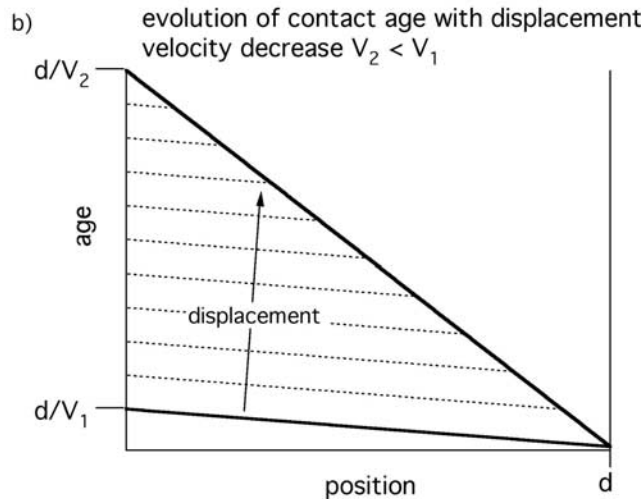
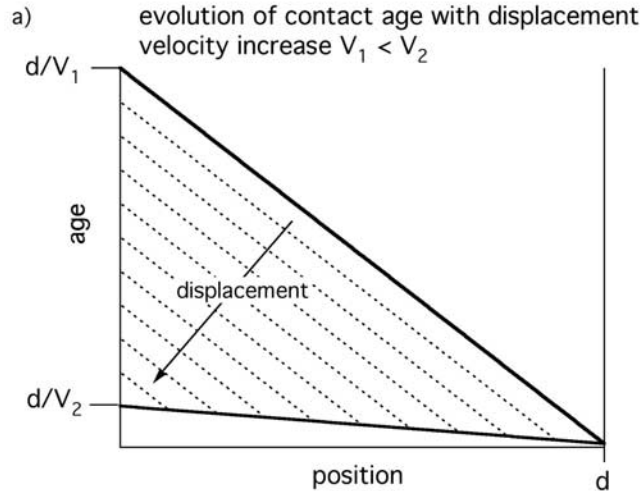


Figure 5. Effect of a distribution of contact sizes on fault strength during steady state sliding. (a) Lognormal distribution of contact sizes, $P(d) = (1/\sigma d\sqrt{2\pi})\exp[-(\ln d - \mu)^2/2\sigma^2]$ with $\mu = 1.44$, $\sigma = 0.58$. Contacts are square and sliding normal to the contact edge. The average contact dimension is $5 \mu\text{m}$, and the standard deviation of the distribution is $10 \mu\text{m}$. (b) Distribution of contact ages for the case shown in Figure 5a with $V = 0.2 \text{ m/s}$. Using $\alpha = 1 \times 10^{-6} \text{ m}^2/\text{s}$, $\rho\hat{c} = 4 \times 10^6 \text{ J/m}^3 \text{ }^\circ\text{K}$, $T_b = 750^\circ\text{C}$, $T_f = 200^\circ\text{C}$, $\tau_c = 3 \times 10^9 \text{ Pa}$, the critical age is $4.2 \times 10^{-5} \text{ s}$ (vertical line). (c) Steady state fault strength (gray) for the contact distribution shown in Figure 5a for a range of sliding velocities with the same parameters as in Figure 5b and assuming $f_w = 0$. Shown for comparison is a corresponding Rice model (equation (5)) with $f_0 = 0.8$, $f_w = 0.0$, and $V_0 = 0.338 \text{ m/s}$ (black). Using the constants listed above in the Rice model corresponds to $d = 5 \mu\text{m}$. Also shown is a fit (dashed) to the fault strength from a distribution of contact sizes using the empirical relation equation (7) with $f_0 = 0.8$, $f_w = 0.0$ (both fixed) and $V_0 = 0.678$.

Using the same lognormal distribution (Figure 5), even for a fairly narrow range of contact asperity dimensions, step changes in sliding velocity lead to a more exponential change of age with displacement and a longer evolution

distance (Figure 7) than for a single contact model. In laboratory experiments where the distribution of contact sizes known, the evolution of age might be estimated directly from (9). To reiterate, rarely is this the case, and even more poorly constrained is the distribution of contact asperity sizes for natural faults.



5. Semiempirical Relationship for Modeling Flash Processes

[14] Conveniently, an existing differential equation for the displacement and time dependence of contact age reproduces the behavior of (9) well under many circumstances. Our requirements for a relationship are average contact age $\theta_{ss} = d/2V$ and a gradual change of age with displacement associated with changes in sliding velocity. These properties are associated with the aging relationship of *Ruina* [1983]

$$\frac{d\theta}{dt} = \left(1 - \frac{V\theta}{d_c}\right), \tag{10}$$

where θ is sometimes referred to as the slowness state variable in the context of rate and state friction. While (10) is empirical, to represent contact age for flash weakening, its use can be justified as follows. First, for flash processes the relationship between contact age and strength (5) has some theoretical basis due to *Rice* [1999] (e.g., equation (4)). Second, the solution of (10) at constant slip speed is exponential which, at least in our example (Figure 7), reproduces the expected evolution of the age of a contact population nearly exactly. In general, for laboratory contact size distributions, numerical tests suggest (10) well represents the evolution of contact age.

[15] Using the steady state equivalence $\theta_{ss} = d_c/V$ and equation (7) we expect that steady and nonsteady state fault strength should follow

$$f = f_w + \frac{f_0 - f_w}{1 + \frac{d_c}{\theta V_0} \left\{ 1 - \exp \left[- \left(\frac{d_c}{\theta V_0} \right)^2 \right] \right\}}. \tag{11}$$

Equations (10) and (11) can be combined to model flash processes during dynamic rupture.

6. Discussion

[16] An obvious application of these models of strength change are to contact-scale melting [*Rice*, 1999] but these

Figure 6. Spatial distribution of contact age with displacement for right lateral slip at constant rate for the single representative square contact model with reference to the lower asperity contact. (a) Velocity increase. Heavy lines represent the initial and eventual steady state age. Dashed lines are the spatial age distribution at nine intermediate displacements. (b) Same as Figure 6a, for a velocity decrease. (c) Changes of average age with displacement for cases shown in Figures 6a and 6b, a step increase (shaded, left-hand axis) and a step decrease (black, right-hand axis).

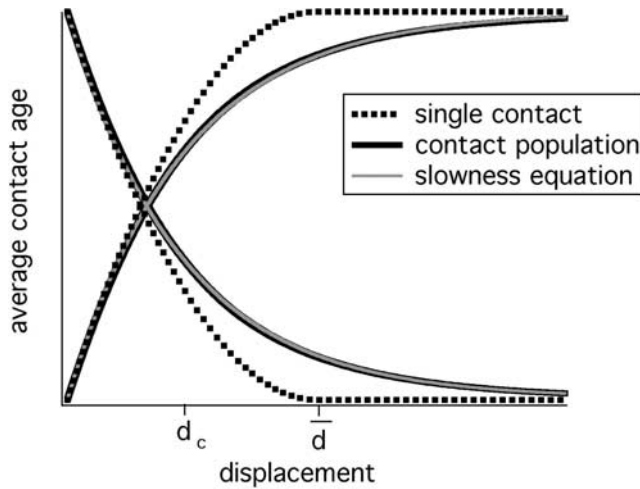


Figure 7. Changes of average age of a lognormal distribution of square contacts (heavy black line) with displacement for step increases and decreases. In this calculation the lognormal distribution (see Figure 5 caption) has $\mu = 1.44$, $\sigma = 0.58$. Contacts are sliding normal to their edges. The average contact dimension \bar{d} is $5 \mu\text{m}$, and the standard deviation of the distribution is $10 \mu\text{m}$. Shown for comparison is the single square contact solution for $d = 5 \mu\text{m}$ (dashed), and the solution to the slowness evolution equation of *Ruina* [1983] for $d_c = 2.3 \mu\text{m}$ (shaded).

equations are equally applicable to other phase transformations and reactions which produce strength change, including increases in strength. Nonmelting breakdown reactions occur due to shear heating, and in the case of dehydration may contribute to the susceptibility to melting during rapid slip. For reference, values of material constants at ambient

conditions (25C, 1 atm) for use in equation (5) for some example minerals are listed in Table 1.

6.1. Estimates of the Slip Velocity Threshold for Weakening

[17] The onset of flash weakening inferred from lab measurements (Figure 4) can be compared with the model predictions of V_0 (4b) which require known breakdown temperature, thermal properties, yield strength and asperity contact dimension. This would be easiest for monomineralic rocks because only a single set of material constants are needed. Average asperity contact size and contact shear strength are reasonably well known or can be estimated [e.g., *Brown and Scholz*, 1985; *Dieterich and Kilgore*, 1996], and mineral thermal properties are very well known. Unfortunately, there only limited (unpublished) data for flash weakening of a single phase rock. Predictions of weakening become much more complicated for rocks with multiple constituent minerals.

[18] For application to melting, studies of pseudotachylite composition [*Spray*, 1993, and references therein] suggest that the onset is controlled by phases with low breakdown temperature, typically amphiboles and sheet silicates. Breakdown of these hydrous phases releases water that generally lowers the melting point of the solid products and of adjacent phases. As a consequence the matrix of frictionally generated melts is water-rich, enriched in metal oxides and depleted in quartz and feldspar relative to the host rock composition, due to the preferential incorporation of hydrous minerals into the melt. Similar arguments may apply for flash melting in some cases; however, generally, the onset of weakening will be limited by the available number of contacts of the phase with the lowest V_0 as estimated from equation (4b). The strongest weakening should coincide with V_0 associated with the most abundant

Table 1. Material Constants and Calculated Thermal Parameters^a

Mineral	T_b , °C	λ , W/m °K	ρ , g/cm ³	W_m , g/mol	f_0	C_p , J/mol °K	V_m , cm ³ /mol	σ_y , GPa	G, GPa	$\rho\hat{c}$, $\times 10^6$ J/m ³ °K	α , m ² /s	α_e , m ² /s
Quartz	1730	4.3	2.65	60.09	0.58	44.6	22.69	10.87	44.3	1.97	2.19×10^{-6}	1.94×10^{-6}
Orthoclase/ microcline	1150	1.35	2.57	278.33		202.4	108.72	7.62	28.1	1.86	7.25×10^{-7}	4.78×10^{-7}
Albite	1100	1.35	2.62	262.23	0.6	205.1	100.07	7.62	28.6	2.05	6.59×10^{-7}	4.81×10^{-7}
Anorthosite	1550	0.85	2.76	78.21		211.4	100.79	7.62	39.9	2.10	4.05×10^{-7}	6.23×10^{-7}
Fosterite	1890	2.96	3.27	140.69	0.74	117.9	43.79	10	81.1	2.69	1.10×10^{-6}	1.59×10^{-6}
Fayalite	1205	4.37	4.37	203.78		132.9	46.39	10	50.7	2.86		
Actinolite	750	1.22	3.15					6.24				
Tremolite	850	2.78	3.15	812.37	0.6	655.63	272.92	6.24		2.40	1.16×10^{-6}	1.02×10^{-6}
Hornblende	750	1.6	3.2					6.24	46.15			
Paragasite	1000		3.25					6.24				
Clinopyroxene-diopside /augite	1400	2.75	3.1	216.55	0.72	166.52	66.09	6.24	61.95	2.52	1.09×10^{-6}	2.04×10^{-6}
Orthopyroxene-enstatite /hypersphene	1425	2.63	3.4	100.39		82.09	31.47	6.91	75.7	2.61	1.01×10^{-6}	1.71×10^{-6}
Muscovite	650	1.3	2.82	398.31	0.38	326.1	140.71	0.8	35.3	2.32	5.61×10^{-7}	4.00×10^{-5}

^aDefinitions, references, notes: T_b , breakdown temperature, *Spray* [1992] and *Robie et al.* [1979]; λ , thermal conductivity, *Clawser and Huenges* [1995] and *Horai* [1971]; ρ , density, *Hurlbut and Klein* [1977]; W_m , molecular weight, *Robie et al.* [1979]; f_0 , friction, friction data for individual rock or mineral types are quite variable, values listed here are representative for the particular study cited: quartzite [*Ruina*, 1980], albite [*Scruggs and Tullis*, 1998], olivine (dunite) (D. L. Goldsby, unpublished data, 2003), amphibole no data used Byerlee's law, pyroxene (gabbro) [*Marone and Cox*, 1994], muscovite [*Scruggs and Tullis*, 1998]; C_p , heat capacity, *Robie et al.* [1979]; V_m , molar volume, *Robie et al.* [1979]; σ_y , indentation hardness, estimated from Mohs hardness [*Hurlbut and Klein*, 1977] (while the yield stress for mineral asperity contacts has not been widely measured in indentation, an empirical relation between Mohs hardness H_m and microindentation hardness σ_y follows from recent experiments of *Broz et al.* [2006]; their tabulated data are fit by $\sigma_y = 0.123 H_m^{2.3}$ (see Figure A1); G , shear modulus, *Bass* [1995]; $\rho\hat{c}$, volumetric heat capacity, calculated from $\rho\hat{c} = C_p/V_m$; α , thermal diffusivity, calculated from $\alpha = \lambda/\rho\hat{c}$; α_e , effective thermal diffusivity for flash heating, calculated from $\alpha_e = V_0 d = \pi\alpha[\rho\hat{c}(T_b - T_f)/S]^2$ (equation (4b)), with $T_f = 25^\circ\text{C}$; S , initial contact shear strength, calculated from $S = f_0\sigma_y$.

minerals. Following *Spray's* [1993] argument that bulk melting is controlled by lithology, some preliminary idea of material control on flash weakening can be gained by considering the effective thermal diffusivity dV_0 . Some estimated values are included in Table 1 (also see Table 1 notes). Complications may arise at two phase contacts, such as eutectic melting at temperatures below T_b of either phase [e.g., *Semenov*, 1995]. However, because frictional melting is nonequilibrium [*Spray*, 1992, 1993; *Shimamoto and Lin*, 1994; *Lin and Shimamoto*, 1998] eutectic melting probably is not significant. A model of weakening for localized slip between multiphase rock surfaces might be constructed from the expected contact composition distributions, but is outside the scope of this paper.

[19] An additional consideration is that rather than an abrupt solid to liquid transition at a threshold melting temperature, melting generally initiates below the melting temperature at free surfaces and grain boundaries where bonding is weakest, crystal structure is disordered or has higher energy [e.g., *Dash*, 2002]. Thus this premelting is expected at asperity contacts and the melting temperatures appropriate for the bulk (e.g., Table 1) likely overestimate the onset of contact melting. However, given the approximate nature of our model and scarce data on premelting for rock forming minerals, we have neglected all aspects of premelting.

[20] For simplicity, here we ignore possible two phase effects, the influence of ambient and dehydration produced water, and premelting at asperity contacts and estimate V_0 for flash weakening of gabbro [*Tsutsumi and Shimamoto*, 1997] using the material properties of the principal constituents pyroxene, feldspar, amphibole at ambient conditions. We do not account for the effect of contact stress on the breakdown temperature which in most cases should increase the melting temperature, perhaps significantly. Taking $d = 1 \times 10^{-6}$ to 10×10^{-6} m we expect the onset of weakening in the range of 0.05 to 2 m/s based on constants in Table 1. Fits to *Tsutsumi and Shimamoto's* [1997] high-speed data are consistent with this estimated threshold (Figure 4a).

[21] Results from high-speed slip of novaculite, a nearly pure fine grained quartz rock, are expected to be better constrained. Again taking $d = 1 \times 10^{-6}$ to 10×10^{-6} m, (5) predicts the onset of weakening in the range of 0.2 to 2 m/s based on constants in Table 1. The observed threshold is at slightly lower velocity (Figure 4b) indicating that the average contact size is somewhat larger than estimated, that estimates of the thermal parameters are off or that other factors we have ignored (premelting) are important.

6.2. Contact-Scale Implications for Shear Melting

[22] While constitutive equations (5), (7), and (10) seem to capture many of the features of weakening attributed to flash heating in lab experiments, published data are limited. In the absence of extensive lab tests we explore implications for contact-scale physics given available data on melt viscosity and asperity contact stress in the context of Rice's original model. If shear heating produces melt at asperity contacts the flash weakening relationship (5d) can be recast using the melt viscosity to define an effective melt thickness by equating the contact shear resistance $\tau_c = f\sigma_y$ to shear resistance due to the presence of a thin melt layer with

viscosity η and thickness w , $\tau_c = \eta V/w$. Replacing f with (5d) leads to a relationship for the effective melt thickness

$$w = \frac{\eta V^2}{\sigma_y[(f_o - f_w)V_0 + V f_w]}, \quad V \geq V_0. \quad (12a)$$

At the onset of melting the slip rate is $V = V_0$, defining a threshold melt thickness

$$w_0 = \frac{\eta V_0}{\sigma_y f_0}. \quad (12b)$$

The physical interpretation of (12b) is that any melt thickness exceeding w_0 will have a shear resistance that is less than the shear yield strength of the solid asperity contacts. To estimate w available viscosity from bulk frictional melting of gabbro ($\eta = 120$ Pa s) [*Hirose and Shimamoto*, 2005] must be corrected to account for differences in the normal stress in those tests (1.5 MPa) and the expected contact normal stresses leading to flash melting (~ 5 GPa). An appropriate viscosity at contacts can be estimated by assuming an Arrhenius pressure dependence

$$\eta = \eta_0 \exp \frac{P \Delta V_\eta}{RT} \quad (13)$$

where η_0 is the viscosity at zero pressure, R is the gas constant, T is temperature in $^\circ\text{K}$ and ΔV_η is the activation volume for melting [e.g., *Tinker et al.*, 2004]. For the limited available data for silicate melts ΔV_η is in the range of -12 to -5×10^{-6} m³/mol [*Tinker et al.*, 2004]. Taking $\Delta V_\eta = -8.9$ m³/mol, and using the case of gabbro for illustration ($V_0 = 0.34$, $f_0 = 0.6$, $\sigma_y = 5 \times 10^9$ Pa) this pressure dependence leads to $\eta = 0.98$ Pa s at 5 GPa. A consequence of the very low viscosity is that the predicted layer thicknesses are very low. The range of expected thicknesses (12a) for gabbro at slip rates up to a few meters per second is no more than a few nanometers; the threshold thickness (12b) is 0.1 nm. These are not plausible because molecular dimensions for pyroxene, feldspar and amphibole are in the range of 5 to 12×10^{-10} m. The minimum melt thickness must be several unit cells, say 2 to 5 nm, as required for shear of a continuous melt layer.

[23] In addition, melt at unconfined asperity contacts will tend to flow out of the contact due to the pressure gradient from the center to the edge of the contact. Taking the contact pressure to be the average contact normal stress, the expected instantaneous velocity of melt extrusion from a contact might be simply estimated as $V_{ex} = \sigma_y w / \eta$. This extrusion rate is of the same order as the shear velocity in (12), implying a thinner melt film than predicted by (12a) and (12b). These issues and definitive measurements of flash melting would be best addressed by careful optical and electron microscopy of asperity contacts recovered from flash heating experiments coupled with determinations of the viscosity and pressure dependence of bulk melts of equivalent composition.

[24] That a viscosity higher than estimated here is required to produce reasonable melt thicknesses suggests

either (1) that flash melting does not result in melts of the same composition as bulk melting, (2) that the viscosity of thin melt films is higher than bulk melts, or (3) that there are additional resistances in the contact region that we have not accounted for. With regard to suggestion 2, higher viscosity is expected for thin melt films because of increased order and bonding within the liquid within a few molecular distances of the solid interface [e.g., *Oxotoby*, 1990; *Dash*, 2002]. As for resistance in the contact region, our simple model of a stationary contact distribution without wear ignores damage, distributed deformation and comminution, known to accompany frictional slip between bare rock surfaces even at low normal stress such as in unconfined tests in the experimental geometry of *Tsutsumi and Shimamoto* [1997] [see *Di Toro et al.*, 2006, supplemental material].

6.3. Depth Dependence of Onset Slip Speed

[25] While the standard expectation is that shear heating increases with depth in the earth because the shear resistance increases with overburden, $\tau = f\sigma$, the contact-scale shear resistance that leads to flash heating does not because the contact shear resistance is fixed $\tau_c = S = f\sigma_y$ by the contact yield stress. Instead, depth dependence of the onset speed arises from two effects: (1) the geothermal gradient increasing T_f in (5d) with depth and (2) from the transient nature of asperity contacts. For the former the onset slip speed will decrease linearly with depth. For the latter, contact has a limited lifetime $\hat{\theta} = d/2V$ (Figure 1) with heat production $Q = SV\hat{\theta} = Sd/2$. Whether or not there is depth dependence to the propensity for flash heating beyond the explicit dependence of T_f on depth depends on whether there are depth-dependent changes in average contact dimension.

[26] Theories of how the characteristic contact dimension changes with overburden are speculative; *Scholz* [1988] suggests dramatic decrease of the characteristic length with increasing depth, based on elastic analysis of contact between surfaces with fractal roughness. In contrast, the friction theory that underlies the present model suggests a weak increase in contact heat production with overburden, as follows. An increase in normal stress with depth produces an increase in either number of contacts or the average area of contact according to $\sigma = n\sigma_y A_c/A$ and for the square contact $A_c = d^2$. So for fixed fault area and number of contacts, the heat produced then varies with the square root of normal stress,

$$Q = SV\hat{\theta} = \frac{S}{2} \sqrt{A \frac{\sigma}{n\sigma_y}}, \quad (14)$$

as opposed to linearly as for bulk melting, $Q = f\sigma V\Delta t$. However, the direct measurement of the normal stress dependence of average contact dimension and the number of contacts on laboratory fault surfaces suggest that the increase of area of individual contacts is nearly exactly counterbalanced by an increase in the number of contacts such that the average contact dimension is essentially independent of normal stress [*Dieterich and Kilgore*, 1996]. This independence of contact dimension on normal stress

can occur when the changes to existing contact dimensions are small and the new contacts are small relative to the mean. This is expected for laboratory samples which are rough at small scale but flat at long wavelengths [*Greenwood and Williamson*, 1966]. Unfortunately, extrapolation of this result to seismic faulting is complicated by large differences in the character of surface roughness between natural and lab surfaces.

[27] Whether or not flash heating effects are important during seismic faulting depends significantly on the average contact dimension. At present the expected size of the characteristic sliding distance for seismic faulting and the average contact dimension for seismic faults are first-order unknowns in source physics. So, we must conclude, based on the theory, that we do not know over what range of seismic slip and source depth flash heating determines fault strength during earthquake faulting.

6.4. Implications for Earthquake Source Properties

[28] Some clues as to whether flash weakening is important might be apparent from comparing the implied earthquake source properties to seismological observations. In the following we consider the dynamic strength determined solely by flash weakening, acknowledging that for large earthquakes other processes (bulk melting, pore fluid pressurization) might also play important roles, especially at the largest displacements [e.g., *Di Toro et al.*, 2006; *Rice*, 2006].

6.4.1. Dynamic Stress Drop

[29] While the onset slip speed may be independent or weakly dependent on fault normal stress, the stress drop should increase linearly with normal stress because of the expected increase in the failure strength [e.g., *Byerlee*, 1978]. Estimate the dynamic stress drop implied by flash weakening by equating it with the strength loss $\Delta\tau_d = \sigma_n (f_0 - f) = \sigma_n (f_0 - f_w) (1 - V_0/V)$ of (5). To consider a representative range of shear stresses in the seismogenic crust, without consideration of tectonic setting, we simply equate fault normal stress with overburden, that is, an effective normal stress gradient of 18 MPa/km. Using $V = 1$ m/s, as appropriate for earthquakes, a depth range of 5 to 15 km, and values of f_0 , f_w , and V_0 from *Tsutsumi and Shimamoto* [1997] (0.8, 0.2, 0.34 m/s) produces a range of dynamic stress drop 40–120 MPa. Although some estimates of local dynamic stress drops are this high [*Bouchon*, 1997], generally, dynamic stress drops are 1 to 20 MPa [e.g., *Kanamori*, 1994]. On the basis of these estimates flash weakening is either not the dominant mechanism controlling earthquake dynamic stress drop, or effective normal stress in the crust is lower than estimated here.

6.4.2. Slip Weakening Distance and Effective Shear Fracture Energy

[30] Assume that the dominant asperity contact size for earthquakes is the same for laboratory faults, noting that caveats about the asperity contact size expressed in section 6.3 also apply to estimates of the slip weakening distance. Allowing for a distribution of contact sizes (Figure 7) suggests d_c in strength evolution relations (10) and (11) is approximately 1/2 the average asperity contact size. From this we estimate the slip weakening distance very approximately as $4d_c$. For lab observations this yields slip weakening distances of 4 to 40 μm .

[31] The effective shear fracture energy is defined as energy per unit area dissipated during strength loss in excess of the minimum strength

$$G_e = \int_0^{d_*} \tau d\delta - \tau(d_*)d_* \quad (15)$$

[Rice, 1980]. A lower bound on G_e for flash weakening is estimated by assuming an instantaneous change in slip speed from V_0 to the maximum speed, here taken to be 1 m/s. Note that the evolution equation (10) is exponential at constant slip speed. While this makes the slip weakening distance somewhat poorly defined, in this particular case the minimum strength, maximum slip and integration limit can be replaced by values associated with ∞ rather than d_* . The fracture energy is

$$G_e = \int_0^{\infty} \tau d\delta - \tau(\infty)d_{\infty} = -\Delta\tau_d d_c \exp\left.\frac{-\delta}{d_c}\right|_0^{\infty} = \Delta\tau_d d_c. \quad (16)$$

The above estimates of $\Delta\tau_d$ and corresponding range of d_c (1 to 10 μm) result in $G_e = 160\text{--}4830 \text{ J/m}^2$. This is a lower bound due to assumption of instantaneous slip speed increase; inertia requires slip speed to increase more gradually with displacement. Better estimates require fully elastodynamic simulations [e.g., *Bizzarri and Cocco*, 2003]. Still, these are very low fracture energies when compared to estimates for large earthquakes and for hazardous earthquakes flash weakening would produce an unusually large proportion of radiated to fracture energy unless the slip weakening distance is much larger than estimated here.

[32] The slip weakening distance in the experiments of Goldsby and Tullis [unpublished] (Figure 4b) is consistent with being controlled by asperity dimensions as in the flash weakening models, though it is not well resolved. Unfortunately, there are problems in interpreting the slip weakening distance in the experiments of *Tsutsumi and Shimamoto* [1997] (Figure 4a) as being related to the asperity contact size. Weakening prior to bulk melting in gabbro experiments conducted at the same conditions as *Tsutsumi and Shimamoto's* [1997] occurs over slip of between one and one half meter [see *Hirose and Shimamoto*, 2005, Figure 2b]. Here the sample circumference (157 mm), the fault length in the direction of sliding, is about 1/3 to 1/6 of the slip weakening distance. Thus the slip weakening distance in these tests is more likely related to the wear necessary to achieve a stable asperity population or to bulk heating of the whole fault surface than it is to the asperity contact size during flash weakening of a stationary contact distribution, as in Rice's flash weakening model.

6.4.3. Static Stress Drop

[33] Static stress drop $\Delta\tau_s$ cannot be reliably estimated from laboratory observations without fully elastodynamic simulations. Fortunately, some work with a constitutive relation with inverse rate dependence, similar to (10) and (11), has been done by *Zheng and Rice* [1998]. These simulations show a strong tendency to produce self-healing slip pulses. Such self-healing is generally expected from (5), (7) or (10) and (11). The self-healing results from the very strong negative rate dependence; decreasing slip speed

behind the rupture front produces a dramatic increase in strength such that the fault becomes stronger than the stress available to drive slip [*Heaton*, 1990]. This mode of rupture propagation will result in undershoot, and $\Delta\tau_s < \Delta\tau_d$. Thus, while flash weakening may produce very large dynamic stress drops, the corresponding static stress drops may be considerably smaller. Simulations to date have not considered rupture arrest rigorously, so it is not possible to quantitatively estimate implied static stress drop at present.

6.5. Problem of Shear Zone Thickness

[34] A significant unknown in our considerations of weakening is the shear zone thickness. In the above analysis, shear deformation presumes a fully localized fault slip surface. If instead fault displacement is accommodated within a shear zone of finite thickness w_f , the slip velocity at a representative contact asperity is $V_c = VD/w_f$ where D is the average grain diameter. Given natural observations of *Chester et al.* [2005] showing relatively thick principal shear zones ($>1 \text{ mm}$) and relatively small mean particle sizes ($72\% < 10 \mu\text{m}$) the contact slip speed could be many times or even orders of magnitude smaller than for the fully localized laboratory fault, in which case flash melting may be suppressed. Some more sophisticated ideas about the degree of localization during shear heating are considered by *Rice* [2006] and *Rempel* [2006].

7. Conclusions

[35] Previous laboratory faulting experiments conducted at high sliding velocities, below the threshold for bulk melting, show dramatic strength reduction consistent with a shear-induced phase change at asperity contacts. Natural faults are expected to have a wide range of asperity contact sizes and a numerical model of flash weakening that allows for arbitrary contact size distributions predicts a gradual onset of weakening. A relatively simple closed-form constitutive equation for flash processes can be used to approximate asperity contact distributions; this semiempirical expression also fits the lab observations well. The lab data for gabbro and for novaculite are consistent with a nonzero limiting strength for flash weakening however this conclusion is not definitive.

[36] At laboratory conditions the expected threshold velocity for weakening is between 0.05 and 2 m/s for gabbro, in qualitative agreement with experimental observations. The model predicted threshold for novaculite is 0.2 to 2 m/s, slightly larger than observed in lab tests. Extrapolation of this model to natural conditions suggests that flash weakening will produce large dynamic stress drop, small effective shear fracture energy and undershoot. These extrapolations and estimates of the natural threshold slip speed are tentative due to poor knowledge of the average contact dimension, shear zone thickness, and fault gouge particle size at seismogenic depths.

Appendix A: Material Properties for Flash Weakening Calculations

[37] The predicted onset of flash weakening from models such as (4) requires breakdown temperature, thermal properties, and yield strength. Published values for select min-



Figure A1. Broz *et al.*'s [2006] data for microindentation hardness σ_y and Mohs hardness H_m . These are well fit by the power law relationship $\sigma_y = Ch_m^n$, and the curve shown as a least squares fit with $C = 0.123$ GPa and $n = 2.3$.

erals are listed in Table 1, following Spray's [1993] compilation of material properties for bulk melting. Yield strength is estimated from Mohs hardness using an empirical relationship inferred from the recent data of Broz *et al.* [2006] (Figure A1).

[38] **Acknowledgments.** This study was supported by USGS Earthquake Hazards program and by the Southern California Earthquake Center through 2002 SCEC grant 02132. This is SCEC contribution 1023. Discussion and correspondence with D. Lockner, G. Di Toro, A. Rempel, T. Shimamoto, and J. Rice are gratefully acknowledged. In particular, J. Rice provided notes of unpublished work, A. Rempel suggested references on premelting and comminution, and T. Shimamoto and G. Di Toro summarized known lab constraints on the composition of frictional melts and provided guidance in interpreting experimental data. The paper was improved in response to comments by J. Andrews, B. Aaggard, A. Rempel, T. Shimamoto, and G. Di Toro.

References

Bass, J. D. (1995), Elasticity of minerals, glasses and melts, in *Mineral Physics and Crystallography: A Handbook of Physical Constants, Ref. Shelf*, vol. 2, pp. 45–63, AGU, Washington, D. C.

Bizzarri, A., and M. Cocco (2003), Slip-weakening behavior during the propagation of dynamic ruptures obeying rate- and state-dependent friction laws, *J. Geophys. Res.*, *108*(B8), 2373, doi:10.1029/2002JB002198.

Bouchon, M. (1997), The state of stress on some faults of the San Andreas system as inferred from near-field strong motion data, *J. Geophys. Res.*, *102*, 11,731–11,744.

Bowden, F. B., and D. Tabor (1950), *The Friction and Lubrication of Solids*, 374 pp., Clarendon, Oxford, U. K.

Brown, S. R., and C. H. Scholz (1985), The closure of random elastic surfaces in contact, *J. Geophys. Res.*, *90*, 5531–5545.

Broz, M. E., R. F. Cook, and D. L. Whitney (2006), Microhardness, toughness and modulus of Mohs scale materials, *Am. Mineral.*, *91*, 135–142.

Byerlee, J. D. (1978), Friction of rocks, *Pure Appl. Geophys.*, *116*, 615–626.

Chester, J. S., F. M. Chester, and A. K. Kronenberg (2005), Fracture surface energy of the Punchbowl Fault, San Andreas System, *Nature*, *437*, 133–136.

Clauser, C., and E. Huenges (1995), Thermal conductivity of rocks and minerals, in *Rock Physics and Phase Relations: A Handbook of Physical Constants, Ref. Shelf*, vol. 3, pp. 105–126, AGU, Washington, D. C.

Dash, J. G. (2002), Melting from one to two to three dimensions, *Contemp. Phys.*, *43*, 427–436.

Dieterich, J. H. (1978), Time-dependent friction and the mechanics of stick-slip, *Pure Appl. Geophys.*, *116*, 790–806.

Dieterich, J. H., and B. D. Kilgore (1996), Imaging surface contacts: Power law contact distributions and contact stresses in quartz, calcite, glass and acrylic plastic, *Tectonophysics*, *256*, 219–239.

Di Toro, G., T. Hirose, S. Nielsen, G. Pennacchioni, and T. Shimamoto (2006), Natural and experimental evidence of melt lubrication of faults during earthquakes, *Science*, *311*, 647–649.

Goldsby, D. L., and T. E. Tullis (2002), Low frictional strength of quartz rocks at subseismic slip rates, *Geophys. Res. Lett.*, *29*(17), 1844, doi:10.1029/2002GL015240.

Greenwood, J. A., and J. Williamson (1966), Contact of nominally flat surfaces, *Proc. R. Soc. London, Ser. A*, *295*, 300–319.

Heaton, T. H. (1990), Evidence for and implication of self-healing pulses of slip in earthquake rupture, *Phys. Earth Planet. Inter.*, *64*, 1–20.

Hirose, T., and T. Shimamoto (2005), Growth of molten zone as a mechanism of slip weakening of simulated faults in gabbro during frictional melting, *J. Geophys. Res.*, *110*, B05202, doi:10.1029/2004JB003207.

Horai, K. (1971), Thermal conductivity of rock-forming minerals, *J. Geophys. Res.*, *76*, 1278–1308.

Hurlbut, C. S., and C. Klein (1977), *Manual of Mineralogy*, 532 pp., John Wiley, Hoboken, N. J.

Kanamori, H. (1994), Mechanics of earthquakes, *Annu. Rev. Earth Planet. Sci.*, *22*, 207–237.

Lin, A., and T. Shimamoto (1998), Selective melting processes as inferred from experimentally generated pseudotachylytes, *J. Asian Earth Sci.*, *16*, 533–545.

Linker, M. F., and J. H. Dieterich (1992), Effects of variable normal stress on rock friction: Observations and constitutive equations, *J. Geophys. Res.*, *97*, 4923–4940.

Marone, C. J., and S. J. D. Cox (1994), Sealing of rock friction constitutive parameters: The effects of surface roughness and cumulative offset on friction of gabbro, *Pure Appl. Geophys.*, *143*, 359–385.

Oxotoby, D. W. (1990), New perspectives on freezing and melting, *Nature*, *347*, 725–730.

Power, W. L., and T. E. Tullis (1992), The contact between opposing fault surfaces at Dixie Valley, Nevada, and implications for fault mechanics, *J. Geophys. Res.*, *97*, 15,425–15,435.

Power, W. L., T. E. Tullis, and J. D. Weeks (1988), Roughness and wear during brittle faulting, *J. Geophys. Res.*, *93*, 15,268–15,278.

Rempel, A. (2006), The effects of flash-weakening and damage on the evolution of fault strength and temperature, in *Radiated Energy and the Physics of Earthquake Faulting*, *Geophys. Monogr. Ser.*, vol. 170, edited by R. Abercrombie *et al.*, pp. 263–270, AGU, Washington, D. C.

Rice, J. R. (1980), The mechanics of earthquake rupture, in *Physics of the Earth's Interior*, edited by A. M. Dziewonski and E. Boschi, *Proc. Int. Sch. Phys. Enrico Fermi*, *78*, 555–649.

Rice, J. R. (1999), Flash heating at asperity contacts and rate-dependent friction, *Eos Trans. AGU*, *80*(46), Fall Meet. Suppl., F681.

Rice, J. R. (2006), Heating and weakening of faults during earthquake slip, *J. Geophys. Res.*, *111*, B05311, doi:10.1029/2005JB004006.

Robie, R. R., B. S. Hemingway, and J. R. Fisher (1979), Thermodynamic properties of minerals and related substances at 298.15 K and 1 bar pressure and at higher temperatures, *U.S. Geol. Surv. Bull.*, *1452*, 456 pp.

Ruina, A. L. (1980), Friction laws and instabilities: A quasi-static analysis of some dry frictional behavior, Ph.D. thesis, 99 pp., Brown Univ., Providence, R. I.

Ruina, A. L. (1983), Slip instability and state variable friction laws, *J. Geophys. Res.*, *88*, 10,359–10,370.

Scholz, C. H. (1988), The critical slip distance for seismic faulting, *Nature*, *336*, 761–763.

Scruggs, V. J., and T. E. Tullis (1998), Correlation between velocity dependence of friction and strain localization in large displacement experiments on feldspar, muscovite and biotite gouge, *Tectonophysics*, *295*, 15–40.

Semenov, A. P. (1995), Tribology at high temperature, *Tribol. Int.*, *28*, 45–50.

Shimamoto, T., and A. Lin (1994), Is frictional melting equilibrium melting, or non-equilibrium melting?, *J. Tectonic Res. Group Jpn.*, *39*, 79–84.

Spray, J. G. (1992), A physical basis for the frictional melting of some rock forming minerals, *Tectonophysics*, *204*, 205–221.

Spray, J. G. (1993), Viscosity determinations of some frictionally generated silicate melts: Implications for fault zone rheology at high strain rates, *J. Geophys. Res.*, *98*, 8053–8068.

Summers, R., and J. Byerlee (1977), Summary of results of frictional sliding studies, at confining pressures up to 6.98 kb, in select rock materials, *U.S. Geol. Surv. Open File Rep.*, *77-142*, 129 pp.

Tinker, D., C. E. Leshner, G. M. Baxter, T. Uchida, and Y. Wang (2004), High-pressure viscometry of polymerized silicate melts and limitations of the Eyring equation, *Am. Mineral.*, *89*, 1701–1708.

Tsutsumi, A., and T. Shimamoto (1997), High-velocity frictional properties of gabbro, *Geophys. Res. Lett.*, *24*, 699–702.

Tullis, T. E., N. M. Beeler, and J. D. Weeks (1993), The nature of the evolution effect in rock friction, *Eos Trans. AGU*, *74*, 296.

Zheng, G., and J. R. Rice (1998), Conditions under which velocity-weakening friction allows a self-healing versus a cracklike mode of rupture, *Bull. Seismol. Soc. Am.*, *88*, 1466–1483.

N. M. Beeler, U.S. Geological Survey, 345 Middlefield Road, MS977, Menlo Park, CA 94025, USA. (nbeeler@usgs.gov)

D. L. Goldsby and T. E. Tullis, Department of Geological Sciences, Brown University, Providence, RI 02912-1846, USA.